

学位論文

Distinct functions between ferrous and ferric iron in lung cancer cell growth
(肺がん細胞増殖における2価鉄と3価鉄の機能差)

日隈 大徳

Hironori Hinokuma

熊本大学大学院医学教育部博士課程医学専攻呼吸器外科学

指導教員

鈴木 実 教授

熊本大学大学院医学教育部博士課程医学専攻呼吸器外科・乳腺外科学

2023年3月

学 位 論 文

論文題名 : **Distinct functions between ferrous and ferric iron in lung cancer cell growth**
(肺がん細胞増殖における2価鉄と3価鉄の機能差)


著者名 : 日隈大徳
Hironori Hinokuma

指導教員名 : 熊本大学大学院医学教育部博士課程医学専攻呼吸器外科・乳腺外科学 鈴木実 教授

審査委員名 :	染色体制御学担当教授	石黒啓一郎
	呼吸器内科学担当教授	坂上拓郎
	細胞医学担当教授	中尾光善
	疾患エピゲノム制御学担当准教授	大口裕人

2023年3月

Distinct functions between ferrous and ferric iron in lung cancer cell growth

Hironori Hinokuma^{1,2} | Yohei Kanamori¹ | Koei Ikeda² | Li Hao¹ | Masataka Maruno¹ | Taishi Yamane¹ | Ayato Maeda¹ | Akihiro Nita¹ | Mayuko Shimoda¹ | Mayumi Niimura¹ | Yuki Takeshima¹ | Shuran Li¹ | Makoto Suzuki² | Toshiro Moroishi^{1,3} 

¹Department of Molecular and Medical Pharmacology, Faculty of Life Sciences, Kumamoto University, Kumamoto, Japan

²Department of Thoracic and Breast Surgery, Graduate School of Medical Sciences, Kumamoto University, Kumamoto, Japan

³Center for Metabolic Regulation of Healthy Aging, Faculty of Life Sciences, Kumamoto University, Kumamoto, Japan

Correspondence

Toshiro Moroishi, Department of Molecular and Medical Pharmacology, Faculty of Life Sciences, Kumamoto University, 1-1-1 Honjo, Chuo-ku, Kumamoto, Kumamoto 860-8556, Japan.
Email: moroishi@kumamoto-u.ac.jp

Funding information

Chugai Foundation for Innovative Drug Discovery Science; Inamori Foundation; Japan Agency for Medical Research and Development (AMED) PRIME, Grant/Award Number: JP22gm6210030; Japan Society for the Promotion of Science (JSPS) KAKENHI, Grant/Award Number: 21H02764; Kobayashi Foundation for Cancer Research; Mochida Memorial Foundation for Medical and Pharmaceutical Research; The Uehara Memorial Foundation

Abstract

Accumulating evidence suggests an association between iron metabolism and lung cancer progression. In biological systems, iron is present in either reduced (Fe^{2+} ; ferrous) or oxidized (Fe^{3+} ; ferric) states. However, ferrous and ferric iron exhibit distinct chemical and biological properties, the role of ferrous and ferric iron in lung cancer cell growth has not been clearly distinguished. In this study, we manipulated the balance between cellular ferrous and ferric iron status by inducing gene mutations involving the FBXL5–IRP2 axis, a ubiquitin-dependent regulatory system for cellular iron homeostasis, and determined its effects on lung cancer cell growth. FBXL5 depletion (ferrous iron accumulation) was found to suppress lung cancer cell growth, whereas IRP2 depletion (ferric iron accumulation) did not suppress such growth, suggesting that ferrous iron but not ferric iron plays a suppressive role in cell growth. Mechanistically, the depletion of FBXL5 impaired the degradation of the cyclin-dependent kinase inhibitor, p27, resulting in a delay in the cell cycle at the G1/S phase. FBXL5 depletion in lung cancer cells also improved the survival of tumor-bearing mice. Overall, this study highlights the important function of ferrous iron in cell cycle progression and lung cancer cell growth.

KEYWORDS

cell cycle, FBXL5, iron, lung cancer, p27

1 | INTRODUCTION

Lung cancer is the second most commonly diagnosed cancer in the world. More than 2 million people worldwide are newly diagnosed with lung cancer each year.¹ Despite recent improvements in treatment strategies, lung cancer remains the most common cause of

cancer-related deaths. Several studies have suggested a link between the dysregulation of iron metabolism and lung cancer progression. Increased serum iron levels have been found in patients with lung cancer.² Further, the deregulated expression of iron-related genes, such as TFR1 and ferritin, has been found in the tumor tissues of patients with NSCLC.³ Based on epidemiological studies, high dietary

Abbreviations: CHX, cycloheximide; FBXL5, F-box and leucine-rich repeat protein 5; FTH1, ferritin heavy chain 1; IRP2, iron regulatory protein; LIP, labile iron pool; LLC, Lewis lung carcinoma; NSCLC, non-small cell lung cancer; PI, propidium iodide; ROS, reactive oxygen species; TFR1, transferrin receptor 1.

This is an open access article under the terms of the [Creative Commons Attribution-NonCommercial](https://creativecommons.org/licenses/by-nc/4.0/) License, which permits use, distribution and reproduction in any medium, provided the original work is properly cited and is not used for commercial purposes.

© 2023 The Authors. *Cancer Science* published by John Wiley & Sons Australia, Ltd on behalf of Japanese Cancer Association.

iron intake and occupational iron exposure are associated with lung cancer risk.^{4,5} Another study also suggested the beneficial role of dietary iron intake on lung cancer risk.⁶ Therefore, the dual functions of iron in lung cancer progression and suppression have been demonstrated in previous studies. However, the precise molecular mechanisms underlying these superficially contradictory functions of iron in lung cancer cell growth remain unclear.

In humans, iron exists in two oxidation states: ferrous iron (Fe^{2+}) and ferric iron (Fe^{3+}).⁷ Iron taken up via TFR1 is released into the cytosol in the ferrous form. Ferrous iron constitutes a cytosolic LIP that is used for direct incorporation into iron-dependent proteins or is routed to the mitochondria, where it is incorporated into heme and iron-sulfur clusters. However, ferrous iron is redox-active and catalyzes the production of ROS via the Fenton reaction, leading to biochemical damage, such as oxidative DNA injury and lipid peroxidation of the cell membrane.^{8,9} To counteract its toxicity, ferrous iron that is not utilized or exported is converted to its ferric form and stored within ferritin. Ferric iron is redox-inactive and must be reduced to the ferrous form prior to entering the LIP. Due to the distinct biological properties of ferrous and ferric iron, the iron valent status and iron amount can contribute to the biological and pathological effects of iron.¹⁰ However, the significance of the iron valent status in lung cancer is unknown.

Cellular iron homeostasis is predominantly regulated by FBXL5 and IRP2.^{11,12} The RNA-binding protein, IRP2, promotes iron uptake and suppresses iron storage and export by regulating the stability and translation of mRNAs encoding proteins responsible for iron metabolism. Accordingly, IRP2 increases cellular ferrous iron levels. Iron-dependent regulation of IRP2 involves iron sensing by FBXL5, which is a substrate recognition component of the SCF E3 ligase complex that mediates the ubiquitination and degradation of IRP2. Under iron-deficient conditions, FBXL5, which is not bound to iron, undergoes proteasomal degradation, which leads to IRP2 accumulation and the consequent upregulation of ferrous iron levels. In contrast, under iron-sufficient conditions, FBXL5 stabilizes and degrades IRP2, thereby downregulating ferrous iron levels. Therefore, the FBXL5-dependent degradation of IRP2 in iron-replete cells is a key event in the maintenance of intracellular iron homeostasis. Disruption of the FBXL5-IRP2 axis causes the dysregulation of ferrous and ferric iron homeostasis. Previously, we revealed that tissue iron levels are higher in FBXL5-deficient and IRP2-deficient mice than in wild-type controls.¹³ Due to constitutive IRP2 accumulation, the amount of ferrous iron was found to increase in FBXL5-deficient mice tissues.¹³ In contrast, IRP2-deficient mice had ferric iron accumulation in several tissues, partly owing to increased iron sequestration by ferritin.^{14,15} In this study, we investigated the distinct roles of ferrous and ferric iron in lung cancer cell growth by genetically manipulating the FBXL5-IRP2 axis. Depletion of FBXL5 but not IRP2 in lung cancer cells suppressed their growth *in vitro*, suggesting that ferrous iron plays a suppressive role in lung cancer cell growth. The *in vivo* tumor growth of FBXL5 KO mouse LLC cells was also suppressed compared to that of WT cells. Mechanistically, the suppression of p27 degradation was identified to be responsible for the delayed G1/S transition in FBXL5 KO cells.

Overall, our results suggest a regulatory role of ferric iron in cell cycle progression and lung cancer cell growth.

2 | MATERIALS AND METHODS

2.1 | Antibody, reagent, and plasmid

Antibodies, reagents, and plasmids are listed in [Tables S1-S3](#).

2.2 | Cell culture and gene deletion

All cell lines were cultured under an atmosphere of 5% CO_2 at 37°C. LLC cells and A549 cells were cultured in RPMI-1640 medium and DMEM, respectively, both supplemented with 10% FBS, penicillin (100 U/mL), and streptomycin (100 mg/mL). The cells were treated with 200 μM ammonium iron (II) sulfate hexahydrate (Fe^{2+}) or 400 μM 2, 2'-bipyridyl (Bpy) for the indicated times. FBXL5, IRP2, and p27 KO cells were generated using the clustered regularly interspaced short palindromic repeats (CRISPR)/Cas9 system. The CRISPR-Cas9 RNA-targeting guide sequences were designed using CRISPOR (<http://crispor.tefor.net/>) ([Table S4](#)). The targeting sequences of mouse FBXL5 and IRP2 were cloned into PX459. The targeting sequences of human FBXL5 and p27 were cloned into plentiCRISPR v2 puro and plentiCRISPR v2 blast, respectively. Both guide sequences of the PX459 plasmids were used for each gene deletion in LLC cells. The PX459 plasmids were transfected into target cells using the Lipofectamine™ 3000 transfection reagent. After puromycin selection, cells were single-cell sorted using a cell sorter (SH800S, Sony), and KO clones were selected via immunoblot analysis. The plentiCRISPR v2 plasmid was used to generate the lentivirus, as described below.

2.3 | Viral infection and overexpression

Human-derived FBXL5 tagged with HA was cloned into the retroviral vector, pBabe puro. The retroviral transfer plasmids were transduced into Platinum-A packing cells using PolyJet™, following the manufacturer's instructions. Lentiviral transfer plasmids were transduced via the co-transfection of pLenti-P2A and pLenti-P2B packaging plasmids into 293T cells using PolyJet™. The medium was changed 12 h after transfection and the supernatant was collected 48 h after transfection. LLC and A549 cells were infected with retrovirus or lentivirus in the presence of 5 $\mu\text{g}/\text{mL}$ polybrene, and selected using puromycin or blasticidin.

2.4 | Mice and tumor models

C57BL/6J mice (female, 8–10 weeks) were used as subcutaneous mouse models. LLC cells (2×10^5) were subcutaneously transplanted

into the back flanks of mice. Tumor size was measured using a caliper every 3 days to calculate the tumor volume ($\text{width}^2 \times \text{height} \times 0.523$). Mice were sacrificed when the tumors reached the maximum allowed size (15 mm in diameter) or when signs of ulceration were evident.

2.5 | Immunoblot analysis

Cells were lysed in lysis buffer (0.5% Triton X-100, 50 mM Tris-HCl pH 7.5, and 150 mM NaCl) with protease inhibitors (10 μ M leupeptin, 1 μ M pepstatin A, and 1 mM phenylmethylsulfonyl fluoride), and the protein concentrations were determined using the Bradford method. Equal amounts of protein extracts were mixed with SDS sample buffer (2.5% SDS, 12.5% glycerol, 87.5 mM Tris/HCl pH 6.8, and 2% 2-mercaptoethanol) and subjected to western blotting analysis. The images were obtained using a ChemiDoc Touch imaging system (Bio-Rad Laboratories).

2.6 | Ferrous iron imaging and measurement

Cells (2×10^4) were cultured for 48 h, washed with HBSS (-), and incubated with FerroOrange at 1:1000 for 30 min. Images were obtained using a BZ-X800 all-in-one microscope (KEYENCE) with a sectioning function. The intensity was quantified from three randomly captured images using the KEYENCE BZ analyzer software. The intensity was extracted from the images and the average intensity per cell was measured. The intensity value was normalized to the mean intensity of the WT.

2.7 | Histological analysis

The tumors were fixed overnight in neutral-buffered formalin. Samples were transferred to 70% ethanol, stored at 4°C until paraffin embedding, and stained with H&E according to standard procedures. For p27 immunostaining, citrate buffer (pH 6.0) with microwaves (5 min \times 3) was used for antigen retrieval. The sections were incubated with 4% block ace powder and p27 antibody (1:50) overnight at 4°C, followed by a secondary antibody for 30 min at room temperature. After the sections were developed using a liquid DAB+ substrate chromogen system for 7 min, the slides were stained with Mayer's hematoxylin. Images were obtained using a BZ-X800. Positive cells were extracted from the images and automatically counted based on the colors of the strongly p27 positive cells using a BZ analyzer.

2.8 | Soft-agar colony formation assay

Lewis lung carcinoma cells (2×10^3) and A549 cells (2×10^3) were cultured in soft agar for 10 days for LLC and 3 weeks for A549 cells,

with the medium being changed every 3 days. The concentrations of the agar gel were 0.4% for the top gel and 0.5% for the basal gel. The colonies were stained with 0.01% crystal violet overnight. Images were obtained and merged into one picture using a BZ-X800, and quantification was performed using a BZ analyzer.

2.9 | 2D growth assay

The cells (1×10^4 cells) were seeded, and cell numbers were counted every 24 h using a Luna™ cell calculator (Logos Biosystems) stained with trypan blue solution.

2.10 | Cell viability assay

The cells (1×10^4 cells) were seeded and collected every 24 h. The collected cells were washed with PBS and stained with PI at 1:10,000. Cell viability was observed using FACS Verse and analyzed using the FlowJo software.

2.11 | Cell cycle assay

Briefly, the cells were labeled with 10 μ M BrdU for 30 min at 37°C before collection. The collected cells were fixed with 70% ethanol and stored at -30°C. The fixed cells were incubated with 2N HCl/0.5% Triton X-100 for 30 min, followed by 0.1 M sodium tetraborate decahydrate treatment for 2 min at room temperature. The cells were then stained with FITC anti-BrdU antibody (1:10) for 30 min at room temperature. After washing, the cells were stained with 1:200 PI. The cell cycle phases were observed using FACS Verse (BD Biosciences) and analyzed using the FlowJo software.

2.12 | CHX chase analysis

The cells were cultured for 16 h, and the medium was changed to a serum-free medium for 24 h to synchronize the cell cycle. The medium was replaced with CHX (100 μ g/mL) and serum-containing medium. The cells were lysed using lysis buffer at the indicated times and prepared for immunoblot analysis. The percentage of p27 and p21 remaining after the indicated incubation times was quantified using ImageJ software.

2.13 | Reverse transcription and quantitative PCR (RT-qPCR) analysis

Total RNA was extracted from cells using TRIzol™, and cDNA was synthesized using the ReverTra® Ace qPCR RT kit, following the manufacturer's protocols. Quantitative PCR was performed using the Luna® Universal qPCR Master Mix. The sequences of the PCR

primers are listed in Table S5. Data were normalized to GAPDH levels and analyzed using the $\Delta\Delta\text{CT}$ method.

2.14 | Analysis of published data

Overall survival (OS) was compared between patients with stage I–IV NSCLC presenting high or low levels of FBXL5 expression in TCGA dataset accessed with the Human Protein Atlas website (<https://www.proteinatlas.org>). The downloaded clinical data (follow-up period and dead or alive status) of patients with stage I–IV NSCLC were evaluated for FBXL5 expression (FPKM value) in tumor tissues and analyzed using the Kaplan–Meier survival method. Data for patients with unknown stages were excluded.

2.15 | Statistical analysis

Statistical analyses were performed using Prism software, version 9.3.1. Quantitative data are presented as mean \pm SD, unless indicated otherwise. Comparisons between two groups were performed using the parametric *t*-test or Mann–Whitney *U*-test. Comparisons among more than three groups were performed using one-way ANOVA, followed by Tukey's multiple comparison test. Comparisons of the time course between the two groups were performed using two-way ANOVA, followed by Bonferroni's multiple comparisons test. Differences between survival curves were analyzed using the log-rank nonparametric test. Statistical significance was set at $p < 0.05$.

3 | RESULTS

3.1 | FBXL5 deletion inhibits anchorage-independent tumor cell growth in vitro

To confirm the regulation of iron valent homeostasis by the FBXL5–IRP2 axis, LLC mouse lung cancer cells were treated with ammonium iron (II) sulfate hexahydrate (Fe^{2+}) or 2, 2'-bipyridyl (Bpy; Fe^{2+} chelator). Consistent with previous studies, accumulation of FBXL5 as well as degradation of IRP2 were evident under ferrous iron-rich conditions, while depletion of ferrous iron leads to FBXL5 degradation and IRP2 accumulation (Figure 1A). These results indicate that FBXL5–IRP2 axis is functional in LLC cells and iron valent homeostasis is physiologically regulated. To investigate the role of ferrous and ferric iron homeostasis in lung cancer, we established FBXL5 KO and IRP2 KO LLC cells using the CRISPR–Cas9 system. It is expected that deletion of FBXL5 causes IRP2 accumulation, leading to an increase in intracellular ferrous iron levels. Conversely, IRP2 deletion may decrease them.¹³ FBXL5 KO cells showed constitutive IRP2 accumulation regardless of ferrous iron conditions. IRP2 negatively regulates the translation of FTH1, which induces the conversion of ferrous iron into ferric iron. FBXL5 KO cells exhibited lower FTH1 expression

than WT cells, whereas IRP2 KO cells exhibited higher expression of FTH1 (Figure 1A). Consequently, ferrous iron levels were increased in FBXL5 KO cells but decreased in IRP2 KO cells (Figure 1B,C). Accordingly, the deletion of FBXL5 or IRP2 is identified to be effective, and these cell lines are appropriate for investigating changes in the balance between ferrous and ferric iron. To determine the effects of ferrous iron on tumor cell growth, we performed a colony formation assay. FBXL5 depletion significantly suppressed anchorage-independent tumor growth in LLC cells, whereas IRP2 depletion did not suppress such growth (Figure 1D,E). FBXL5 depletion also suppressed the anchorage-independent growth of A549 human lung adenocarcinoma cells (Figure S1A,B). Furthermore, the overexpression of exogenous FBXL5 ameliorated the accumulation of IRP2 (Figure 2A), decreased expression of FTH1 (Figure S1C), as well as ferrous iron accumulation (Figure 2B,C) in FBXL5 KO cells, indicating that the reduced expression of FBXL5 is responsible for ferrous iron accumulation in FBXL5 KO cells. Importantly, FBXL5 overexpression compromised the growth suppression of FBXL5 KO cells (Figure 2D,E). To explore whether the accumulation of ferrous iron, in a manner distinct from FBXL5 depletion, reproduces the growth disadvantage observed in FBXL5 KO cells, we generated FTH1 KO LLC cells (Figure S1D). Deletion of FTH1 hindered anchorage-independent tumor growth in LLC cells (Figure S1E). Collectively, these results indicate that ferrous iron homeostasis, governed by the FBXL5–IRP2 axis, is important for lung cancer cell growth in vitro. Notably, FBXL5 deletion and the consequent ferrous iron accumulation suppressed tumor growth of LLC lung cancer cells.

3.2 | FBXL5 depletion suppresses lung cancer cell growth in vivo

To determine the effects of ferrous iron accumulation on tumor growth in vivo, WT or FBXL5 KO LLC cells were subcutaneously injected into the back flank of C57BL/6 mice. Consistent with the results of the colony formation assay in vitro, the deletion of FBXL5 inhibited lung cancer cell growth in vivo (Figure 3A). FBXL5 KO tumors weighed significantly less than WT tumors (Figure 3B). Although no apparent differences in cell morphology were observed between WT and FBXL5 KO tumors, necrotic areas were evident in the central region of WT tumors, possibly due to tumor overgrowth (Figure 3C). Moreover, the survival of mice implanted with FBXL5 KO LLC cells was significantly longer than that of mice injected with WT cancer cells (Figure 3D). To determine whether FBXL5 is associated with prognosis in human lung cancer, we examined FBXL5 mRNA expression in stage I–IV NSCLC patients from TCGA database. Kaplan–Meier survival analysis revealed that low FBXL5 expression was associated with better prognosis in patients with NSCLC. The 5-year OS rates of the low FBXL5 group and high FBXL5 groups were 54% and 42%, respectively ($p < 0.05$) (Figure 3E). Taken together, these results indicate that strict control of ferrous iron homeostasis by FBXL5 plays a pivotal role in lung tumor growth.

FIGURE 1 FBXL5 depletion inhibits anchorage-independent tumor cell growth in vitro. (A) Immunoblot analysis of WT, FBXL5 KO, and IRP2KO are shown. Cells were treated with Fe²⁺ 200 μM or Bpy 400 μM for 3 h. (B) Representative images of intracellular ferrous iron levels measured by FerroOrange. Bars, 50 μm. (C) The average ferrous iron level per cell in each cell type. *****p* < 0.0001 (one-way ANOVA followed by Tukey's multiple comparison test). (D) Representative images of soft-agar colony formation assay. (E) The colony forming areas are presented as the mean ± SD. ****p* < 0.001, n.s.: not significant (*p* > 0.05) (one-way ANOVA followed by Tukey's multiple comparison test).

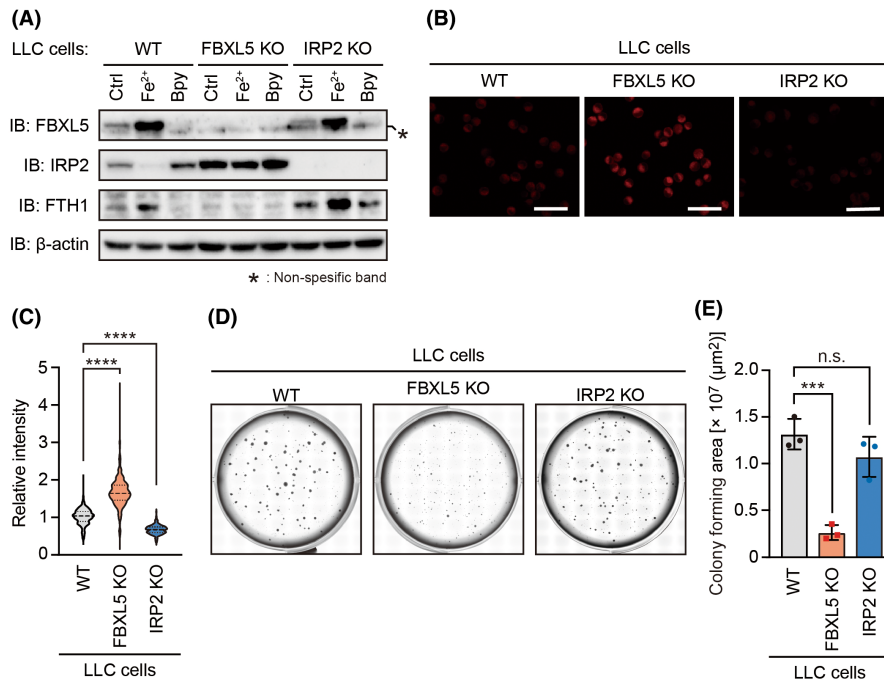
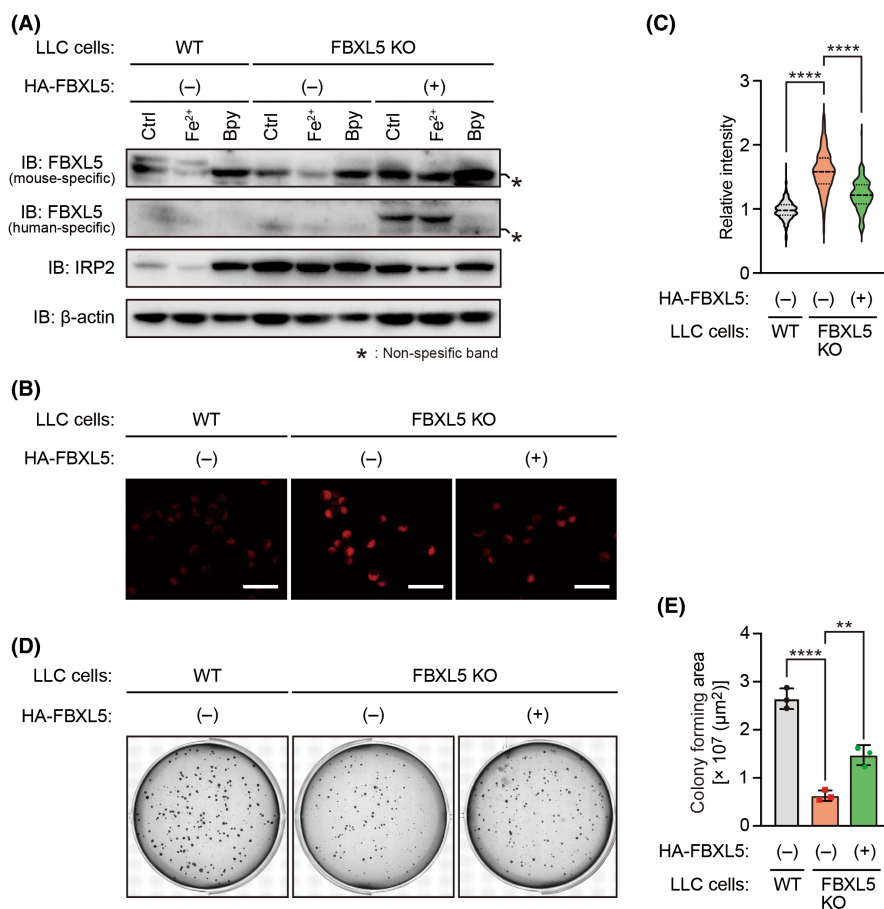


FIGURE 2 HA-tagged FBXL5 reduced ferrous iron levels and recovered tumor cell growth. (A) Immunoblot analysis of WT, FBXL5 KO, and FBXL5 KO + HA-tagged FBXL5 cells are shown. (B) Representative images of intracellular ferrous iron levels detected by FerroOrange. Bars, 50 μm. (C) The average of ferrous iron levels in each cell type was quantified. *****p* < 0.0001 (One-way ANOVA followed by Tukey's multiple comparison test). (D) Representative images of soft-agar colony formation assay. (E) Colony forming areas are presented as the mean ± SD. ***p* < 0.01, *****p* < 0.0001 (one-way ANOVA followed by Tukey's multiple comparison test).



3.3 | G1/S transition is delayed in FBXL5 KO cells

We proceeded to explore the cause of the reduced tumor growth in FBXL5 KO LLC cells. Accordingly, we counted the cell numbers of WT and FBXL5 KO cells together with their viability every 24 h

under regular two-dimensional (2D) culture conditions. The growth of FBXL5 KO cells was markedly suppressed under 2D conditions (Figure 4A), while cell viability was comparable between WT and FBXL5 KO cells (Figure 4B). These results suggest that FBXL5 depletion may impair cell proliferation but not the viability of LLC cells.

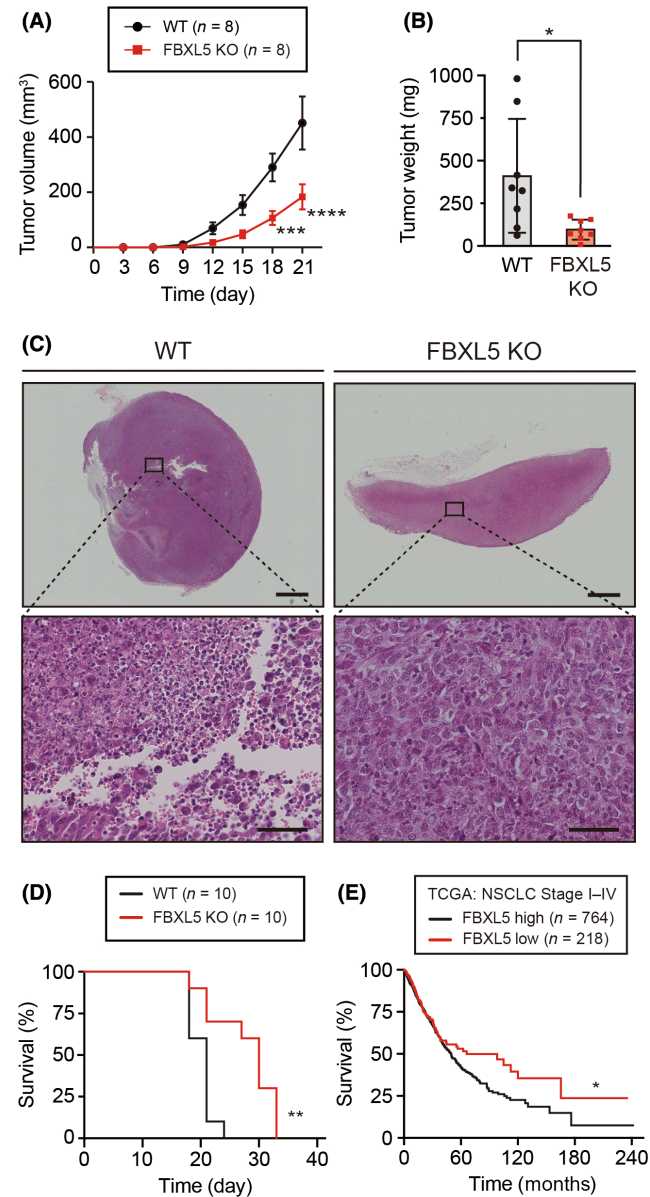


FIGURE 3 FBXL5 depletion suppresses tumor cell growth in vivo. (A) Tumor growth curves. Data are presented as mean \pm SEM; $n=8$ tumors for each group. *** $p < 0.001$, **** $p < 0.0001$ (Two-way ANOVA test followed Bonferroni's multiple comparisons test). (B) Tumor weight. Data are presented as mean \pm SD; $n=8$ tumors for each group. * $p < 0.05$ (Mann-Whitney U -test). (C) H&E images. Bars: 1 mm for the whole picture and 50 μ m for HPF (20 \times magnification). (D) Kaplan-Meier survival curves for tumor-bearing mice ($n=10$ mice per group). ** $p < 0.01$ (log-rank test). (E) Overall survival curves for patients with stage I-IV NSCLC from TCGA dataset with high FBXL5 expression ($n=764$) or low FBXL5 expression ($n=218$) are shown. The cutoff value for FPKM was 14.12. * $p < 0.05$ (Log-rank test).

Therefore, we focused on the effect of FBXL5 depletion on cell cycle progression. BrdU-PI double staining was performed to assess the cell cycle phase distribution. FBXL5 KO cells exhibited increased numbers of cells in the G0/G1 phase and decreased numbers of cells in the S phase compared with WT cells (Figure 4C), implying that the

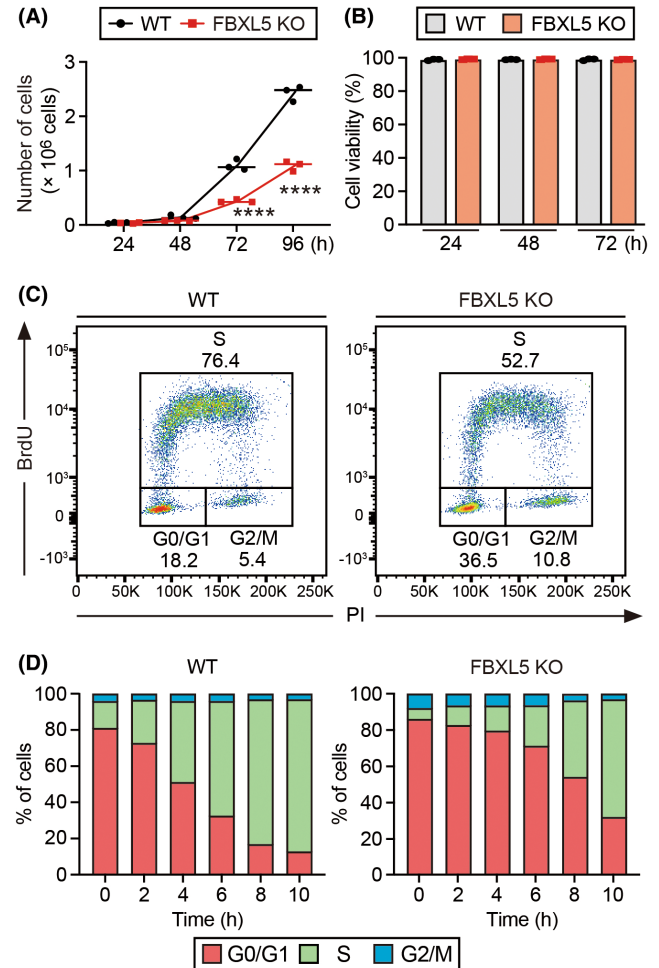


FIGURE 4 G1/S transition is delayed in FBXL5 KO cells. (A) Growth curves of 2D culture. Data are presented as the mean \pm SD. **** $p < 0.0001$ (two-way ANOVA with Bonferroni's multiple comparisons test). (B) Cell viability. Data are presented as the mean \pm SD. Unpaired parametric t -test. (C) Cell cycle analysis. The percentage of cells in the G1, S and G2/M phases. (D) Cell cycle analysis after synchronization by serum starvation.

G1/S transition is impaired in FBXL5 KO cells. When a further evaluation was performed, cells were found to be synchronized at the G1 phase by serum starvation for 24h, and were released into the S phase by replacing the medium with a serum-containing medium. After serum starvation, most cells in both cell lines were arrested in the G1 phase. Time-course analysis revealed that the G1/S transition was delayed in the FBXL5 KO cells (Figure 4D). These findings indicate that the deletion of FBXL5 disturbs the G1/S transition, thereby suppressing lung cancer cell growth.

3.4 | P27 degradation is suppressed during G1/S transition in FBXL5 KO cells

We aimed to identify the molecular mechanism underlying G1/S delay in FBXL5 KO cells. The retinoblastoma protein (Rb)-adenoviral early region 2 binding factor (E2F) pathway integrates

signals to control G1/S transition in the mammalian cell cycle.^{16,17} E2F transcription factors induce the expression of numerous genes required for cell cycle entry and DNA synthesis. Rb forms a complex with E2F to suppress its transcriptional activity.¹⁷ Upon phosphorylation of Rb, E2F is released from the complex, leading to the induction of its transcriptional activity. Based on the mRNA expression of *Ccne1* (also known as Cyclin E1), a representative target of E2F, E2F transcriptional activity was increased rapidly in WT cells, and slowed in FBXL5 KO cells after serum stimulation (Figure 5A). Furthermore, phosphorylation of Rb, a step before E2F activation, also increased over time in WT cells, but was delayed in FBXL5 KO cells (Figure 5B). Rb is phosphorylated by several cyclins and cyclin-dependent kinases (CDKs). CDK inhibitor (CKI) families, including p27 (also known as Kip1) and p21 (also known as Cip1/Waf1), bind to the cyclin-CDK complex and suppress their catalytic activity for Rb phosphorylation.¹⁷ p27 expression was found to remain higher in FBXL5 KO cells than in WT cells after serum stimulation (Figure 5B). In contrast, p21 expression was lower in FBXL5 KO cells than in WT cells. Immunohistochemical

analysis using subcutaneous tumor samples revealed that LLC tumors depleted of FBXL5 displayed a marked increase in p27 levels compared to WT tumors (Figure 5C,D). Taken together, these results suggest that p27 accumulation is associated with reduced Rb phosphorylation and G1/S delay in FBXL5 KO LLC cells.

We proceeded to explore the mechanism underlying p27 accumulation in FBXL5 KO cells. There was no difference in the p27 mRNA levels between FBXL5 KO and WT cells under serum-starved conditions (Figure 5E). To assess the stability of the p27 protein during the G1/S transition, we performed a CHX chase analysis. Following serum stimulation, marked degradation of p27 was evident within 2 h in WT cells; however, FBXL5 KO cells took approximately 4 h to degrade p27 to similar levels (Figure 5F). The delay in p27 degradation was not caused by non-specific downregulation of proteasomal activity as there was no difference in the degradation speed of p21.

Taken together, these findings indicate that the suppression of the G1/S transition by FBXL5 deletion is associated with impaired p27 degradation.

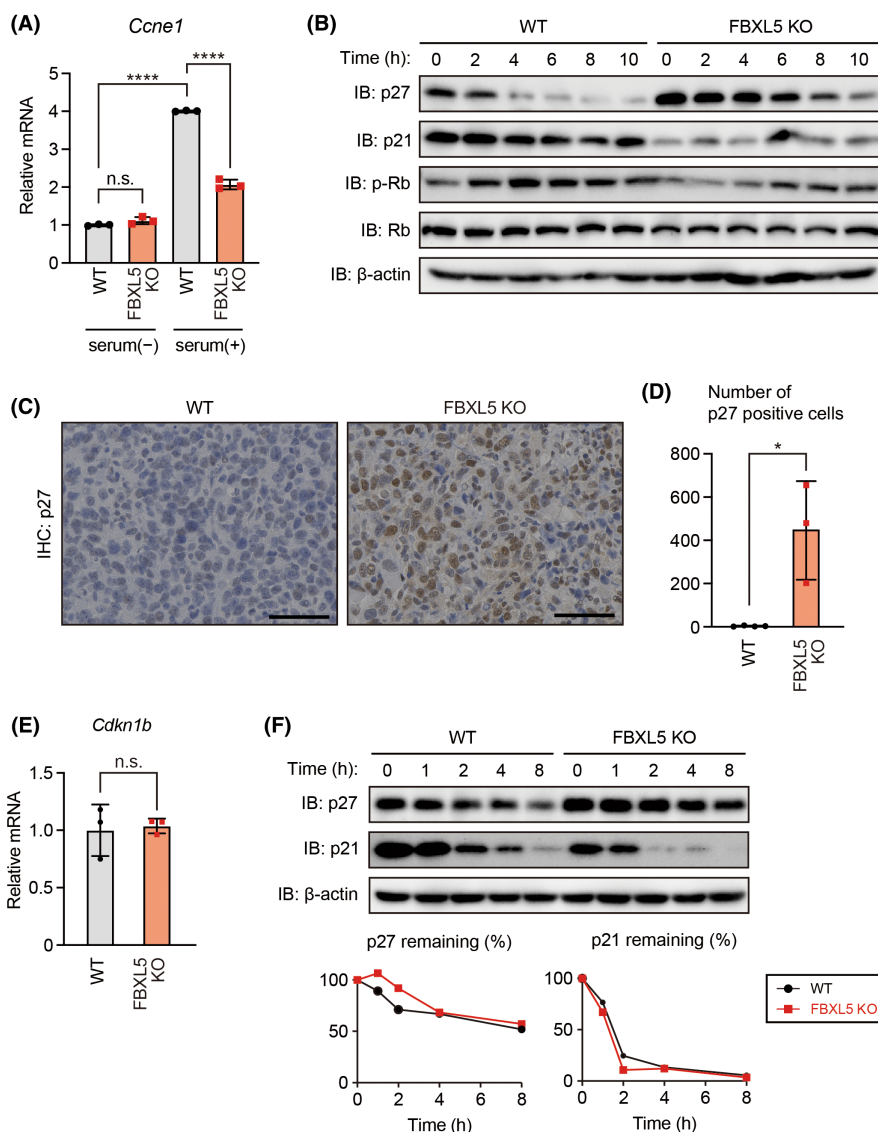


FIGURE 5 p27 degradation is suppressed during G1/S transition in FBXL5 KO cells. (A) mRNA expression level of *ccne1*. Data are expressed as the mean \pm SD. **** $p < 0.0001$, n.s.: not significant ($p > 0.05$) (One-way ANOVA followed by Tukey's multiple comparison test). (B) Immunoblot analysis after serum starvation are shown. (C) Immunohistochemistry images of paraffin-embedded tumors stained with p27. Bars, 50 μ m. Quantification of p27 strong positive cells in three randomly selected fields. Data are presented as the mean \pm SD ($n = 4$). * $p < 0.01$ (Unpaired parametric t-test). (D) The p27 mRNA level under serum starvation are presented as the mean \pm SD. (E) CHX chase assay and the percentage of p27 remaining are shown.

3.5 | p27 accumulation is responsible for growth suppression of FBXL5 KO cells

As p27 degradation was compromised during the G1/S transition in FBXL5 KO cells, we hypothesized that p27 accumulation was responsible for the growth suppression of FBXL5 KO cells. To test this hypothesis, we generated FBXL5/p27 double KO (dKO) LLC cells using the CRISPR-Cas9 system. RB phosphorylation during the G1/S transition was suppressed in FBXL5 KO cells, but markedly increased in FBXL5/p27 dKO cells (Figure 6A). The colony formation assay also revealed that growth suppression by FBXL5 depletion was partially abolished in FBXL5/p27 dKO cells (Figure 6B,C). These results indicate that p27 accumulation is responsible for growth suppression of FBXL5 KO LLC cells. In summary, aberrant ferrous iron homeostasis caused by the loss of FBXL5 suppresses lung cancer cell growth by delaying the cell cycle through p27 accumulation. Our results also highlight an association between the ferrous iron status and G1/S transition.

4 | DISCUSSION

Numerous studies have suggested an association between iron metabolism and lung cancer progression. However, the pathophysiological role of iron in lung cancer remains unclear. Previous studies have mainly focused on the effect of total iron amount on cancer cell growth. The iron chelator, deferasirox, potently inhibits the growth of lung carcinoma xenografts.¹⁸ Iron chelator

treatment decreases expression of cyclin D1 and CDK4, thereby triggering G1 arrest and growth suppression of cultured tumor cells.^{19–21} Moreover, depletion of intracellular iron by ferroportin overexpression induces G1 arrest in prostate cancer cells.²² Accordingly, iron is necessary for efficient G1/S transition and cancer cell growth. Consistent with these findings, we observed a decrease in Cyclin D1 and CDK4 levels in LLC cells when treated with the ferrous iron chelator Bpy (Figure S2A). In contrast, the expression of Cyclin D1 and CDK4 in FBXL5 KO cells remained unchanged. These data suggest that the mechanism underlying the growth suppression triggered by FBXL5 depletion differs from the mechanism triggered by iron chelation, even though both conditions induce G1/S arrest. Our data highlight the significance of the regulation of iron valence by the FBXL5–IRP2 axis in lung cancer progression through the accumulation of p27. As loss of p27 expression is associated with poor OS in patients with NSCLC,²³ a strong correlation was found between p27 and cancer development. However, the mechanism by which iron valency modulates p27 expression in cancer cells remains unclear. Elucidating the detailed mechanism of p27 regulation, including the involvement of IRP2 and ROS downstream of FBXL5, is an important direction for future research.

Although this study highlights the tumor-promoting role of FBXL5 in lung cancer, we previously demonstrated the tumor-suppressive role of FBXL5 in liver carcinogenesis.¹⁰ Genes annotated as “E2F target” and “mitotic spindle” were upregulated in FBXL5-deficient liver tumors, suggesting accelerated cell cycle progression in FBXL5-deficient liver tumors. Furthermore, decreased FBXL5 expression is associated with poor prognosis in patients with hepatocellular carcinoma. FBXL5 plays a tumor-suppressive role by inhibiting epithelial-to-mesenchymal transition (EMT) and cisplatin resistance in gastric cancer.^{24,25} In contrast, FBXL5 promotes cell proliferation and tumorigenesis in colon cancer by modulating PTEN-PI3K/AKT/signaling.²⁶ The exact reason for the opposite role of FBXL5 in cancer is unknown; however, this evidence implies that FBXL5 controls tumor growth in a tissue- and cell type-specific manner. Considering the role of ferritin in iron storage and ferroxidase activity, tumor ferritin levels may be hypothesized to be associated with different effects of FBXL5 depletion on tumor growth among cancer types. Indeed, FBXL5 KO LLC cells displayed reduced ferritin levels (Figure 1A), whereas liver-specific FBXL5-deficient mice exhibited higher hepatic ferritin levels relative to control mice, despite an increase in hepatic IRP2 levels.¹³ In addition to IRP2-mediated translational regulation, ferritin expression is transcriptionally regulated by oxidative stress and inflammation.²⁷ Thus, a comparison of the contribution of FBXL5-dependent and FBXL5-independent regulation of ferritin expression in various cancers would serve as an important future assessment.

Our data showed that FBXL5 depletion in lung cancer cells improved the survival of tumor-bearing mice. A lower expression of FBXL5 was also associated with a better prognosis in NSCLC patients (Figure 3E). Previous studies have shown that ascorbate

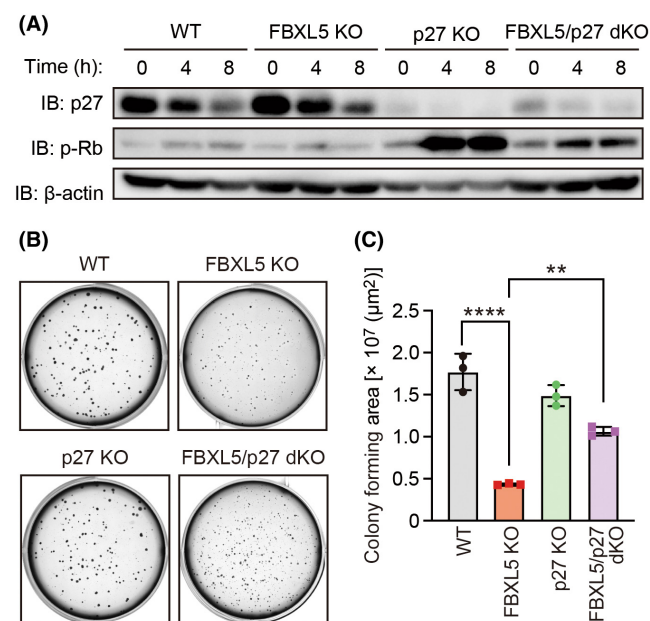


FIGURE 6 p27 is responsible for tumor growth suppression in FBXL5 KO cells. (A) Immunoblot analysis after serum starvation are shown. (B) Representative images of soft-agar colony formation assay. (C) Quantification data for the colony forming areas are presented as the mean \pm SD. ** $p < 0.01$, **** $p < 0.0001$ (one-way ANOVA followed by Tukey's multiple comparison test).

improves the response to chemotherapy for ovarian cancer and pancreatic cancer, and enhances cancer cell-selective radiosensitivity in NSCLC and glioblastoma.^{28,29} As ascorbate increases ferrous iron levels in cancer cells,²⁹ these clinical studies suggest the potential of ferrous iron for improving anticancer therapy. Indeed, increasing intracellular ferrous iron levels are closely associated with ferroptosis, a new form of programmed cell death driven by iron-dependent lipid peroxidation.³⁰ As the induction of ferroptosis has been reported to enhance the efficacy of chemotherapy and radiotherapy,^{31,32} targeting FBXL5 to increase intracellular ferrous iron may be beneficial for the future development of lung cancer treatment. Elucidating the distinct functions of ferrous and ferric iron in tumor development and progression will have important clinical implications in the treatment of lung cancer.

AUTHOR CONTRIBUTIONS

H. Hinokuma: Conceptualization, Data curation, Formal Analysis, Investigation, Validation, Visualization, Writing – original draft, Writing – review & editing. **Y. Kanamori:** Data curation, Formal Analysis, Investigation, Project administration, Supervision, Visualization, Writing – original draft, Writing – review & editing. **K. Ikeda:** Project administration, Supervision, Writing – review & editing. **H. Li:** Data curation, Writing – review & editing. **M. Maruno:** Data curation, Writing – review & editing. **T. Yamane:** Resources, Writing – review & editing. **A. Maeda:** Resources, Writing – review & editing. **A. Nita:** Methodology, Writing – review & editing. **M. Shimoda:** Methodology, Writing – review & editing. **M. Niimura:** Resources, Writing – review & editing. **Y. Takeshima:** Resources, Writing – review & editing. **S. Li:** Resources, Writing – review & editing. **M. Suzuki:** Project administration, Supervision, Writing – review & editing. **T. Moroishi:** Conceptualization, Formal Analysis, Funding acquisition, Methodology, Project administration, Resources, Supervision, Visualization, Writing – original draft, Writing – review & editing.

ACKNOWLEDGMENTS

The authors thank T. Yamauchi, A. Yoshida and other laboratory members for technical assistance and discussion; Core Laboratory for Medical Research and Education, Kumamoto University School of Medicine, for their technical support; and F. Zhang for lentiCRISPR v2.

FUNDING INFORMATION

Financial support: This work was supported by the Japan Society for the Promotion of Science (JSPS) KAKENHI (grant 21H02764), Japan Agency for Medical Research and Development (AMED) PRIME (grant JP22gm6210030), Mochida Memorial Foundation for Medical and Pharmaceutical Research, Kobayashi Foundation for Cancer Research, The Uehara Memorial Foundation, Inamori Foundation, and Chugai Foundation for Innovative Drug Discovery Science to TM.

CONFLICT OF INTEREST STATEMENT

The authors declare no conflict of interest.

ETHICS STATEMENTS

Approval of the research protocol by an Institutional Reviewer Board: N/A.

Informed Consent: N/A.

Registry and the Registration No. of the study/trial: N/A.

Animal Studies: The animal experiments were approved by the Kumamoto University Animal Experiment Committee and conducted in accordance with the laws and regulations concerning animal experiments, animal care and keeping standards, and basic guidelines.

ORCID

Toshiro Moroishi  <https://orcid.org/0000-0001-6419-3882>

REFERENCES

- Sung H, Ferlay J, Siegel RL, et al. Global cancer statistics 2020: GLOBOCAN estimates of incidence and mortality worldwide for 36 cancers in 185 countries. *CA Cancer J Clin.* 2021;71(3):209-249.
- Sukiennicki GM, Marciniak W, Muszynska M, et al. Iron levels, genes involved in iron metabolism and antioxidative processes and lung cancer incidence. *PLoS One.* 2019;14(1):e0208610.
- Kukulj S, Jaganjac M, Boranic M, Krizanac S, Santic Z, Poljak-Blazi M. Altered iron metabolism, inflammation, transferrin receptors, and ferritin expression in non-small-cell lung cancer. *Med Oncol.* 2010;27(2):268-277.
- Fonseca-Nunes A, Jakszyn P, Agudo A. Iron and cancer risk—a systematic review and meta-analysis of the epidemiological evidence. *Cancer Epidemiol Biomarkers Prev.* 2014;23(1):12-31.
- Huang X. Iron overload and its association with cancer risk in humans: evidence for iron as a carcinogenic metal. *Mutat Res.* 2003;533(1-2):153-171.
- Muka T, Kraja B, Ruiter R, et al. Dietary mineral intake and lung cancer risk: the Rotterdam Study. *Eur J Nutr.* 2017;56(4):1637-1646.
- Pantopoulos K, Porwal SK, Tartakoff A, Devireddy L. Mechanisms of mammalian iron homeostasis. *Biochemistry.* 2012;51(29):5705-5724.
- Winterbourn CC. Toxicity of iron and hydrogen peroxide: the Fenton reaction. *Toxicol Lett.* 1995;82-83:969-974.
- Keyer K, Imlay JA. Superoxide accelerates DNA damage by elevating free-iron levels. *Proc Natl Acad Sci U S A.* 1996;93(24):13635-13640.
- Muto Y, Moroishi T, Ichihara K, et al. Disruption of FBXL5-mediated cellular iron homeostasis promotes liver carcinogenesis. *J Exp Med.* 2019;216(4):950-965.
- Salahudeen AA, Thompson JW, Ruiz JC, et al. An E3 ligase possessing an iron-responsive hemerythrin domain is a regulator of iron homeostasis. *Science.* 2009;326(5953):722-726.
- Vashisht AA, Zumbrennen KB, Huang X, et al. Control of iron homeostasis by an iron-regulated ubiquitin ligase. *Science.* 2009;326(5953):718-721.
- Moroishi T, Nishiyama M, Takeda Y, Iwai K, Nakayama KI. The FBXL5-IRP2 axis is integral to control of iron metabolism in vivo. *Cell Metab.* 2011;14(3):339-351.
- LaVaute T, Smith S, Cooperman S, et al. Targeted deletion of the gene encoding iron regulatory protein-2 causes misregulation of iron metabolism and neurodegenerative disease in mice. *Nat Genet.* 2001;27(2):209-214.
- Galy B, Ferring D, Minana B, et al. Altered body iron distribution and microcytosis in mice deficient in iron regulatory protein 2 (IRP2). *Blood.* 2005;106(7):2580-2589.
- Kent LN, Leone G. The broken cycle: E2F dysfunction in cancer. *Nat Rev Cancer.* 2019;19(6):326-338.

17. Rubin SM, Sage J, Skotheim JM. Integrating old and new paradigms of G1/S control. *Mol Cell*. 2020;80(2):183-192.
18. Lui GY, Obeidy P, Ford SJ, et al. The iron chelator, deferasirox, as a novel strategy for cancer treatment: oral activity against human lung tumor xenografts and molecular mechanism of action. *Mol Pharmacol*. 2013;83(1):179-190.
19. Kulp KS, Green SL, Vulliet PR. Iron deprivation inhibits cyclin-dependent kinase activity and decreases cyclin D/CDK4 protein levels in asynchronous MDA-MB-453 human breast cancer cells. *Exp Cell Res*. 1996;229(1):60-68.
20. Liang SX, Richardson DR. The effect of potent iron chelators on the regulation of p53: examination of the expression, localization and DNA-binding activity of p53 and the transactivation of WAF1. *Carcinogenesis*. 2003;24(10):1601-1614.
21. Nurtjahja-Tjendraputra E, Fu D, Phang JM, Richardson DR. Iron chelation regulates cyclin D1 expression via the proteasome: a link to iron deficiency-mediated growth suppression. *Blood*. 2007;109(9):4045-4054.
22. Deng Z, Manz DH, Torti SV, Torti FM. Effects of ferroportin-mediated iron depletion in cells representative of different histological subtypes of prostate cancer. *Antioxid Redox Signal*. 2019;30(8):1043-1061.
23. Hommura F, Dosaka-Akita H, Mishina T, et al. Prognostic significance of p27KIP1 protein and ki-67 growth fraction in non-small cell lung cancers. *Clin Cancer Res*. 2000;6(10):4073-4081.
24. Vinas-Castells R, Frias A, Robles-Lanuza E, et al. Nuclear ubiquitination by FBXL5 modulates Snail1 DNA binding and stability. *Nucleic Acids Res*. 2014;42(2):1079-1094.
25. Wu W, Ding H, Cao J, Zhang W. FBXL5 inhibits metastasis of gastric cancer through suppressing Snail1. *Cell Physiol Biochem*. 2015;35(5):1764-1772.
26. Yao H, Su S, Xia D, et al. F-box and leucine-rich repeat protein 5 promotes colon cancer progression by modulating PTEN/PI3K/AKT signaling pathway. *Biomed Pharmacother*. 2018;107:1712-1719.
27. Alkhateeb AA, Connor JR. The significance of ferritin in cancer: anti-oxidation, inflammation and tumorigenesis. *Biochim Biophys Acta*. 2013;1836(2):245-254.
28. Ma Y, Chapman J, Levine M, Polireddy K, Drisko J, Chen Q. High-dose parenteral ascorbate enhanced chemosensitivity of ovarian cancer and reduced toxicity of chemotherapy. *Sci Transl Med*. 2014;6(222):222ra18.
29. Schoenfeld JD, Sibenaller ZA, Mapuskar KA, et al. O₂(-) and H₂O₂-mediated disruption of Fe metabolism causes the differential susceptibility of NSCLC and GBM cancer cells to pharmacological ascorbate. *Cancer Cell*. 2017;32(2):268.
30. Stockwell BR, Friedmann Angeli JP, Bayir H, et al. Ferroptosis: a regulated cell death nexus linking metabolism, redox biology, and disease. *Cell*. 2017;171(2):273-285.
31. Pan X, Lin Z, Jiang D, et al. Erastin decreases radioresistance of NSCLC cells partially by inducing GPX4-mediated ferroptosis. *Oncol Lett*. 2019;17(3):3001-3008.
32. Li Y, Yan H, Xu X, Liu H, Wu C, Zhao L. Erastin/sorafenib induces cisplatin-resistant non-small cell lung cancer cell ferroptosis through inhibition of the Nrf2/xCT pathway. *Oncol Lett*. 2020;19(1):323-333.

SUPPORTING INFORMATION

Additional supporting information can be found online in the Supporting Information section at the end of this article.

How to cite this article: Hinokuma H, Kanamori Y, Ikeda K, et al. Distinct functions between ferrous and ferric iron in lung cancer cell growth. *Cancer Sci*. 2023;114:4355-4364. doi:[10.1111/cas.15949](https://doi.org/10.1111/cas.15949)